

To appear in ApJ

FU Orionis - The MIDI/VLTI Perspective¹

S. P. Quanz, Th. Henning, J. Bouwman, Th. Ratzka, Ch. Leinert

Max Planck Institute for Astronomy, Königstuhl 17, 69117 Heidelberg, Germany

quanz@mpia.mpg-hd.de

ABSTRACT

We present the first mid-infrared interferometric measurements of FU Orionis. We clearly resolve structures that are best explained with an optically thick accretion disk. A simple accretion disk model fits the observed SED and visibilities reasonably well and does not require the presence of any additional structure such as a dusty envelope. The inclination and also the position angle of the disk can be constrained from the multibaseline interferometric observations. Our disk model is in general agreement with most published near-infrared interferometric measurements. From the shape and strength of the 8-13 μ m spectrum the dust composition of the accretion disk is derived for the first time. We conclude that most dust particles are amorphous and already much larger than those typically observed in the ISM. Although the high accretion rate of the system provides both, high temperatures out to large radii and an effective transport mechanism to distribute crystalline grains, we do not see any evidence for crystalline silicates neither in the total spectrum nor in the correlated flux spectra from the inner disk regions. Possible reasons for this non-detection are mentioned. All results are discussed in context with other high-spatial resolution observations of FU Ori and other FU Ori objects. We also address the question whether FU Ori is in a younger evolutionary stage than a classical TTauri star.

Subject headings: Accretion Disks – Techniques: Interferometric – Circumstellar Matter – Stars: Formation – Stars: Pre-Main Sequence – Stars (Individual): FU Orionis

¹Based on observations made with ESO Telescopes at the Paranal Observatories under program ID 074.C-0209 and 274.C-5032

1. Introduction

FU Orionis is the prototype of a small, but quite remarkable class of low-mass Young Stellar Objects (YSOs) normally referred to as FU Ori objects (FUORs). For the first members of this class an outburst in optical light of up to 4-6 magnitudes over short time scales, followed by a decrease in luminosity over several years or decades, was observed (Herbig 1977). Other objects were included in the class as they shared common specific spectroscopic features, e.g., double-peaked line profiles, a spectral type varying with wavelength and often CO bandhead absorption features. As for one object (V1057 Cyg) the pre-outburst spectrum is known and as it resembles that of a classical TTauri star (Welin 1971), it is commonly assumed that FUORs should be low-mass YSOs. Most observational data can be explained by the presence of an accretion disk surrounding the young stars (Herbig et al. 2003, however, found that some spectral properties are well explained in the context of rapidly rotating late-type stars with strong stellar winds). A dramatic temporal increase in the accretion rate, where the disk outshines the star by several orders of magnitude, can account for the observed outbursts in luminosity. Several scenarios, possibly triggering such an increased accretion rate, have thus far been proposed. They include (a) interactions of binary or multiple systems where tidal forces disturb the circumstellar disk (Bonnell & Bastien 1992), (b) planet-disk interactions, where thermal instabilities in the disk are caused by the presence of a massive planet (Lodato & Clarke 2004), or (c) thermal instabilities in the disk alone (Bell et al. 1995). For a detailed overview concerning the FU Ori phenomenon we refer to Hartmann & Kenyon (1996). Apart from revealing the mechanism leading to the observed outbursts, it is also important to investigate whether all TTauri stars undergo such epochs of enhanced accretion or whether FUORs are a special class of YSOs. Most observations of classical TTauri stars show that the derived accretion rates of $10^{-10} - 10^{-7} M_{\odot}/yr$ (e.g., Gullbring et al. 1998) are not sufficient to build up a low-mass star over time scales of a few Myr. Even if part of the matter is supposed to be accreted in the very early phases of a YSO, FUOR-phases might provide an elegant solution to this problem as they would speed up the accretion process.

As so far only a dozen or so well established FUORs are known and as the FUOR-phase has significant impact on the young star-disk system it is crucial to combine as much observational information as possible for these objects to eventually derive a coherent theoretical picture. Based on near-infrared (NIR) and/or mid-infrared (MIR) interferometry as a technique to study the inner few AU of the accretion disks new insights to some of the best studied FUORs were provided recently. Millan-Gabet et al. (2006) found that accretion disks alone can not reproduce the SED and observed low K-band visibilities for V1057 Cyg, V1515 Cyg and Z CMa-SE simultaneously. They concluded that additional uncorrelated flux may arise due to scattering by large dusty envelopes. Ábrahám et al. (2006) presented the first

VLTI/ MIDI observations of V1647 Ori whose eruptive behavior suggests that it is either an FUOR or an EX Lupi (EXor) type object. In this case it was possible to fit both, the SED and the observed MIR visibility with a simple disk model with moderate disk flaring. For FU Ori itself it was Malbet et al. (2005) who analyzed a wealth of NIR interferometric data. They showed that the NIR visibilities and the SED could be fitted with two models: One consisting simply of an optically thick and geometrically thin accretion disk and a second one consisting of an accretion disk and an embedded "hot spot". From their error statistics these authors concluded that the latter model was more likely.

In summary it becomes clear that up to now no coherent picture can be derived from the interferometric observations of FUORs and the group of objects seems to be rather inhomogeneous.

In this paper we present the first MIR interferometric measurements of FU Orionis. The data are thus complementary to the NIR observations of Malbet et al. (2005). In section 2 we briefly describe the observations and the data reduction process. In section 3 we discuss the findings derived from the N-band acquisition images. The 8-13 μ m spectrum of FU Ori is analyzed in section 4. In sections 5 and 6 we discuss the results from the interferometric measurements, i.e. the visibilities and the correlated flux spectra, respectively. A simple analytical disk model and its fit to the SED and the visibilities is presented in section 7. Finally, we summarize our conclusions and mention some future prospects in section 8.

2. Observations and Data Reduction

The observations were carried out between October 31st and November 4th 2004 with the Mid-Infrared Interferometric Instrument (MIDI) at ESO's Very Large Telescope Interferometer (VLTI) on Paranal/Chile. Together with the Keck Interferometer Nuller that recently started to produce first scientific results (Mennesson et al. 2005), MIDI is currently worldwide the only instrument able to conduct spectrally resolved interferometric observations in the mid-infrared (Leinert et al. 2004). For the observations MIDI was used in high-sens mode using the NaCl prism as dispersive element yielding a spectral resolution of 30. The maximum projected baseline was 86.25m and the minimum projected baseline 44.56m leading to an angular resolution at 10 μ m of 0."/029 and 0."/056, respectively. For an assumed distance of 450 pc these values correspond to 13.1 AU and 25.2 AU. A journal of the observations including projected baselines, position angles and calibrator stars is given in Table 1. For completeness we also mention the observations from December 2004 although they are disregarded in the following sections. These observations had almost exactly the same baseline and position angle as the October observations but showed in general a lower

level of total and correlated flux due to rather poor observing conditions in terms of seeing and transparency. The calibrator stars for the data reduction were chosen by analyzing all calibrator stars observed over the whole night. We selected those showing a good agreement in their transfer functions, i.e. their instrumental visibilities after the assumed sizes were taken into account.

The data reduction was carried out with the software package MIA+EWS-1.3. This software consists of two independent reduction programs (MIA and EWS) which were both applied for comparison. The software, further information and manuals can be downloaded from the Internet². A general description of the basic data reduction steps is also given in Leinert et al. (2004) and we refer the reader to this paper. As the results derived with MIA and EWS agreed quite well (overall differences in the correlated flux $\leq 8\%$), we decided to show only plots resulting from the MIA package.

3. The MIDI Acquisition Image

FU Ori was found to be a binary system by Wang et al. (2004). Reipurth & Aspin (2004) confirmed the detected companion and concluded that it was a young star of spectral type K showing clear NIR excess. In the same paper it was also stated that it was very unlikely that the binary component (FU Ori S) triggered the outburst of FU Ori observed in the late 1930s.

Knowing about the existence of the fainter companion the integration time of some MIDI acquisition images was increased in order to derive N-band photometry for both components. In three images FU Ori S was clearly visible (Figure 1) and aperture photometry could be applied to the observations. The results are summarized in Table 2. Interestingly, FU Ori S shows relatively a higher N-band excess than FU Ori itself. This can be explained in terms of differences in the geometry of an assumed circumstellar disks (e.g., larger flaring angle or smaller disk inclination). We furthermore derive a separation between the components of $0.^{\circ}484 \pm 0.^{\circ}01$ and a position angle of $162.5^{\circ} \pm 4.1^{\circ}$ (measured from north eastwards) which is in good agreement with the results from Wang et al. (2004) and Reipurth & Aspin (2004). Our errors are standard deviations based on Gaussian fitting of 3 independent images. For an assumed distance of 450 pc the separation corresponds to 217.8 ± 4.5 AU.

²<http://www.strw.leidenuniv.nl/~nevec/MIDI/index.html>

4. The Total Uncorrelated MIR Spectrum

4.1. Comparison to *Spitzer* observations

Figure 2 shows the MIR spectrum of FU Ori. The spectrum obtained with MIDI is the average over the first three observing nights using both Unit Telescopes (UTs). For comparison *Spitzer IRS* data are plotted additionally. Those data were available from the *Spitzer* Data Archive. For the data reduction we used the *droopres* intermediate data product processed through the SSC pipeline S12.0.2. The SMART reduction package developed by the IRS Instrument Team at Cornell (Higdon et al. 2004) was used to extract the spectrum. Within the error bars the spectra agree quite well. A broad and weak silicate emission feature is present between 8-13 μ m. However, the averaged MIDI spectrum appears to be a little flatter than the more roundish *Spitzer* spectrum.

4.2. Possible dust composition

In contrast to other YSOs the observed silicate emission feature of FU Ori is rather weak (see also Hanner et al. 1998). Such a broad and flat MIR dust spectrum can be explained by grains that already underwent some coagulation process (Bouwman et al. 2001). To test this hypothesis we derived a possible dust composition by fitting a dust model to the normalized and continuum subtracted *Spitzer* spectrum from 6-13 μ m. This analysis method is similar to approaches that were successfully applied in previous studies for determining the dust composition of observed dust emission features of other YSOs (e.g., Bouwman et al. 2001). In the model we assume that the observed emission can be computed from the sum of the emission of individual dust species. The species we used are summarized in Table 3 together with references for their optical properties. We furthermore took into account different grain sizes as for each of the dust species the opacities were calculated for 0.1, 1.5, and 6.0 μ m sized particles. To estimate the possible contribution of Polycyclic Aromatic Hydrocarbons (PAHs) to the emission we used a template spectrum based on profiles that were derived from observations (Peeters et al. 2002; van Diedenhoven 2004). Finally, in order to reproduce the observed spectrum we fitted the following emission model to the *Spitzer* data using a least square minimization

$$F_\nu - B_\nu(T_{\text{cont}})C_0 = B_\nu(T_{\text{dust}}) \left(\sum_{i=1}^3 \sum_{j=1}^5 C_{i,j} \kappa_\nu^{i,j} \right) + C_{\text{PAH}} I_\nu^{\text{PAH}} \quad . \quad (1)$$

Here, F_ν is the observed flux, $B_\nu(T_{\text{cont}})$ denotes the Planck function at the temperature of the underlying continuum, $B_\nu(T_{\text{dust}})$ the Planck function at the temperature of the silicate

grains, $\kappa_{\nu}^{i,j}$ is the mass absorption coefficient for the silicate species j with the grain size i , I_{ν}^{PAH} is the template emission spectrum for the PAHs, and C_0 , $C_{i,j}$, and C_{PAH} are the weighting factors for the continuum, the silicate emission and the PAH contribution, respectively. A more detailed description of the dust model and plots showing the different dust opacities is given in Bouwman et al. (2006).

The model results are shown in Figure 3 and Table 4 summarizes the corresponding dust composition. As for the underlying continuum we could fit a temperature of 880 K, we believe that this optically thick emission most likely arises from the inner parts of the disk close to the star. The outer and thus cooler regions of the disk would then be responsible for the weak silicate emission for which we fitted a temperature of 230 K to the optically thin emission layer. The results strongly support the idea that most particles are amorphous and much larger in size than those in the ISM. PAHs, silica particles and crystalline silicates do not seem to be present at all. Although the derived fractions of different dust species do depend on the model applied to the data (e.g., in terms of the precise grain sizes considered and also in terms of particle structures) the main conclusions, that we do not find evidence for crystalline silicates and that the grains are considerably larger than those found in the ISM, remain unaltered. For a more detailed discussion about the influence of different model parameters we refer to Voshchinnikov et al. (2006) and van Boekel et al. (2004).

As the disk is much brighter in the optical and NIR than the central star (section 7), stellar radiation is probably not able to produce the observed weak emission feature in an optically thin disk surface layer. However, it was shown that the silicate feature of FU Ori can be reproduced taking into account self-irradiation of the disk (Lachaume 2004). In this case the hot inner parts of the accretion disk serve as flux source and illuminate the disk surface layer under a certain angle.

5. The Visibilities

In Figure 4 and Table 5 the visibilities measured for FU Ori at three different baselines are shown. The errors are computed as standard deviations resulting from the use of different calibrators for each night (see Table 1). In most of the following plots the position of the atmospheric ozone band is indicated as this part of the spectrum suffered sometimes from imperfect corrections during the data reduction process. Here, small “dips” and “bumps” in otherwise flat spectra are remnants from the data reduction.

5.1. Qualitative assessment

The calibrated visibility of the shortest baseline (UT2-UT3) remains almost constant at ≈ 0.95 over the whole wavelength range and the source is only marginally resolved. As expected, for the longest baseline (UT2-UT4) the lowest visibility is observed ranging from ≈ 0.73 at $8.3\mu\text{m}$ to ≈ 0.6 at $13\mu\text{m}$. For the intermediate baseline (UT3-UT4) the visibility shows a slight increase from ≈ 0.73 at $8.3\mu\text{m}$ to ≈ 0.85 at $13\mu\text{m}$. The fact that the object is clearly resolved with two baselines in the MIR supports the argument of Malbet et al. (2005) that we are observing an extended circumstellar structure, i.e. a disk, and not only the stellar photosphere (Herbig et al. 2003).

For the two baselines UT2-UT3 and UT2-UT4 the observations are consistent with expectations from thermal disk emission as despite the decreasing resolution for longer wavelengths the visibilities indicate larger sizes for the emitting regions (see also section 5.3.). The observed increase in visibility for the UT3-UT4 baseline implies that for this baseline, however, the object appears smaller at $13\mu\text{m}$ than at $8\mu\text{m}$. This seems difficult to imagine in the context of a circumstellar disk as emitting source and certainly a second observation for this baseline configuration seems eligible. Theoretically it is possible that the photometric measurements carried out directly after the interferometric observations are corrupted due to technical problems or different weather conditions. This in turn might then lead to a change in the visibility function. However, the calibrators observed at this night did not show any sign of poor photometric measurements and their transfer function was very stable over the whole night. In addition, also other YSOs with circumstellar disks showed an increasing visibility for certain baselines when observed with MIDI. Thus, since we do not find any evidence for excluding this dataset due to bad quality we decided to keep it in our analyses.

5.2. Comparison to MIR visibilities of HAeBe stars

As thus far no MIDI visibilities for TTauri stars have been published we are limited to a comparison between FU Ori and circumstellar disks around Herbig Ae/Be stars (HAeBes). It shows that these stars as well as models applied to them normally show a prominent drop in the visibility between $8\mu\text{m}$ and $10\mu\text{m}$ from where the curve remains almost constant (Leinert et al. 2004). Qualitatively, this drop results from the intensity distribution of the passive disks around the HAeBes: At the short wavelength end the hot inner rim of the disks provides an overproportional contribution to the flux and is at the same time confined to a small spatial region leading to a high visibility. Most of the rest of the MIR emission originates from a large area of the hot, illuminated surface layer of the flared circumstellar disk. The visibilities for FU Ori show hardly any wavelength dependence and are very flat

from 8-13 μm regardless of baseline. Thus, it seems as if the flux distribution of FU Ori is smoother and the visibilities show no sign of a significant contribution from a hot inner rim. However, as FU Ori is surrounded by a heavily active accretion disk where the disk alone produces the majority of the observed flux at almost all wavelengths (see section 7) differences in the intensity distribution and thus in the visibility can be expected.

Apart from differences in the shape of the visibility curves most HAeBes are much better resolved, i.e. show lower visibilities than FU Ori (Leinert et al. 2004). This, however, can at least partly be explained by the distance to these objects which is in general less than 200 pc. FU Ori on the other hand has an assumed distance of 450 pc, and if it was closer to the Earth we would observe lower visibilities also for this object.

5.3. Geometry of the emitting regions

To derive a simple model for the geometry of the emitting regions we assume a simple Gaussian brightness distribution for each baseline. This is a reasonable first approximation for objects showing high visibilities. The FWHM, and hence the physical size, of this Gaussian in arcsec can be computed by

$$\Theta = \sqrt{\frac{\ln(V(f))}{-3.56 \cdot f^2}} \quad (2)$$

where $V(f)$ is the measured visibility for a certain spatial frequency $f = \frac{B}{\lambda}$ (in arcsec^{-1}) derived from the projected baseline B and the wavelength λ . Equation 2 results from a simple Fourier transformation of the assumed brightness distribution. We computed the FWHM for all three baselines at three different wavelengths (9.0, 11.0, and 12.5 μm). For this we averaged for each baseline 5 visibility points from Table 5 centered on the specified wavelengths. Table 6 gives the resulting sizes of the emitting regions in AU for an assumed distance to FU Ori of 450 pc. The results are also visualized in Figure 5 where the FWHM are shown in their orientation on the sky. As expected for thermal disk emission the FWHM increases with wavelength for a given baseline. The only exception is the 12.5 μm size for the UT3-UT4 baseline which is surprisingly a little smaller than that seen at 11.0 μm .

In addition to size estimations for each individual baseline our measurements based on different position angles allow to constrain the geometry of the disk. We fitted the derived FWHM with an ellipse for each of the considered wavelengths in order to derive a simple model for the spatial orientation of an assumed disk-like structure. The resulting best fit ellipses are overplotted in Figure 5 and their parameters are summarized in the lower half of Table 6. As one would expect from a disk-like structure showing a decrease in temperature

with radius the semimajor axes of the ellipses increase with wavelength. However, due to the increasing visibility of the UT3-UT4 baseline the semiminor axis and also the total area of the ellipse are slightly smaller at $12.5\mu\text{m}$ than at $11.0\mu\text{m}$.

An inclination angle for an assumed circular disk can be derived by computing the \arccos of the ratio of the semiminor and semimajor axis. The resulting angles agree very well ($55.4^\circ \pm 2.4^\circ$) and are also in good agreement to what was found for FU Ori disk models based on NIR observations (Malbet et al. 2005). By combining the derived inclination angle with rotational velocity measurements in the optical spectral region it is possible to estimate the central mass. Based on Kenyon, Hartmann & Hewett (1988) we derive for FU Ori $M/M_\odot \approx 0.36$ which is reasonably consistent with typical values for low-mass pre-main sequence stars.

In addition to the inclination the fitted ellipses provide also information on the position angle of the disk. The position angles (measured from north eastwards) we find for the semimajor axes at different wavelengths show a larger scatter ($109.1^\circ \pm 11.6^\circ$) than the inclinations and differ significantly from the NIR findings of Malbet et al. (2005) (see also section 7). It seems as if the position angle becomes smaller for longer wavelengths, although one has to keep in mind that, again, at least for the UT3-UT4 baseline the increasing visibility is the main reason for the observed rotation. At this point we leave it to future investigations to derive a 3-D disk model based on a more complex dust distribution possibly able to confirm the apparent changes in the position angle for different wavelength regimes.

6. The Correlated MIR Spectra

6.1. The origin of the correlated flux

The correlated flux is directly linked to the total flux (i.e. the flux from a single UT telescope) via the visibility:

$$F_{corr}(\lambda) = V(\lambda) \cdot F_{total}(\lambda) \quad (3)$$

Figure 6 depicts the results for the correlated flux for the three different baselines. The total spectrum is plotted for comparison.

Taking into account the spatial resolution of the three baselines it is possible to estimate from where the correlated $8\text{-}13\mu\text{m}$ flux originates. Our UT2-UT3 baseline has a spatial resolution of ≈ 25 AU at the distance of FU Ori, and if we assume an average visibility of 0.95 we hence know that 95% of the $8\mu\text{m}\text{-}13\mu\text{m}$ flux must come from within this 25 AU. Similarly, we find that for the UT2-UT4 baseline 65% of the flux is emitted from the inner

13 AU. For the UT3-UT4 baseline 75% of the 8-13 μ m flux comes from the inner 20 AU.

6.2. Lacking crystalline silicates?

The spatially resolved MIR spectra of the MIDI instrument make it possible to study the radial dependence of the dust composition in the protoplanetary disk (van Boekel et al. 2004). In section 4 we showed that the spatially unresolved (total) spectrum of FU Ori can be fitted with mainly large amorphous dust grains. The shape of the spatially resolved (correlated) flux spectra contains information about the dust composition of the inner parts of the disk.

To compare the shape of the correlated spectra to the total spectrum we first subtracted the continuum for which we fitted a straight line between the flux at 8.25 and 12.95 μ m. Then we normalized all continuum subtracted correlated flux spectra and the total *Spitzer* spectrum by

$$F_{norm} = \frac{F_{sub}}{F_{mean,sub}} \quad (4)$$

where F_{sub} and $F_{mean,sub}$ denote the continuum subtracted spectra and their mean value, respectively. By applying this formula all correlated spectra conserve their shape and can be compared to the total spectrum (Figure 7). To identify those parts where the spectra differ significantly we furthermore computed the deviation from the total *Spitzer* spectrum for each wavelength in units of the data error:

$$\sigma_{dev} = \frac{F_{norm,corr} - F_{norm,total}}{\sigma_{corr}} \quad (5)$$

$F_{norm,corr}$ and $F_{norm,total}$ are the normalized correlated spectra and the normalized total spectrum and σ_{corr} denotes the standard deviation of the correlated spectra (MIDI errors) at a given wavelength. We applied the same normalization factors to the errors as we did to the spectra. Figure 7 shows that no clear deviations from the total unresolved spectrum are observed for any of the correlated spectra. This means that with the given spatial resolution and sensitivity no significant chemical difference in the dust composition is observed and the spectra of the inner parts of the disk look very similar to the total unresolved disk spectrum.

This finding is somewhat surprising. As seen in section 4 the silicate dust grains apparently already underwent noticeable coagulation. Thus, the disk does not consist of purely ISM dust anymore and must already have a significant age. In addition it is known that apart from grain growth also thermal annealing takes place within protoplanetary disks and transform the amorphous silicates into crystalline silicates (see, Henning et al. 2006; van

den Ancker 2000). However, neither the total spectrum nor the correlated spectra indicate the presence of crystalline silicates. This is even more surprising considering the high temperatures in the disk interior due to viscous heating of this actively accreting star (section 7). Annealing processes transforming ISM amorphous dust into crystalline dust set in in disk regions where $T \geq 800K$ (e.g., Gail 2004). In addition to that, high accretion rates directly relate to a faster vertical and horizontal mixing within the protoplanetary disk (Gail 2001). This effect also eases the detection of crystalline silicates within the accretion disk surrounding FU Ori. But why don't we find any evidence for their existence?

A possible explanation might be that they simply cannot be detected as the related feature is rather weak and simply dominated by the underlying continuum. This hypothesis can be checked by analyzing the longer wavelength regime of the *Spitzer* spectrum as shown in Figure 8. As at longer wavelengths the temperature of the continuum is decreasing the contrast between the continuum and possible emission features due to the presence of crystalline silicate particles increases. Hence, spectral signatures of these particles should be more easily detectable. Figure 8, however, shows that also between 14 and $34\mu\text{m}$ the spectrum of FU Ori does not show any clear signs of crystalline silicates. Normally crystalline forsterite particles have emission bands at 16.4, 23.9, 27.7 and $33.8\mu\text{m}$ and enstatite grains show features at 18.8, 21.5, and $24.5\mu\text{m}$ (Molster & Kemper 2005). If one argued that possibly around $27.7\text{-}27.8\mu\text{m}$ a weak forsterite feature was present one should keep in mind that the features at 23.9 and $33.8\mu\text{m}$ are normally stronger (Min et al. 2005) but are not seen at all. Thus, also the longer wavelength MIR spectrum of FU Ori shows that crystalline silicates are not present. This shows that apparently the non-detection is at least not only due to contrast problems between the emission features and the underlying continuum.

What else can prevent us from detecting crystalline silicates? In case FU Ori underwent its first (of possible multiple) outburst(s) and phase(s) of enhanced accretion, it is possible that not enough time has yet elapsed for the crystalline silicate particles to reach the disk surface from where they can be detected by means of MIR spectroscopy. This hypothesis is, however, questionable as the large sizes of the amorphous silicates indicate that enough time, at least for dust coagulation, has elapsed. Recently, Dullemond, Apai & Walch (2006) found that assuming the crystallization by thermal annealing happens at the very early phases of disk evolution, the level of crystallinity is linked to the properties of the molecular cloud core from which the disk formed. It was found that rapidly rotating cores produce rather massive disks with a high accretion rate but a low level of crystallinity. As we observe these properties for FU Ori the proposed model, although yet very simple and with limited predictive power, might provide an interesting way to explain at least partly the lack of crystalline silicates in the FU Ori accretion disk. Finally, another possibility might be that the vertical and radial mixing within the disk does not work as efficient as expected. In consequence not enough

crystalline dust grains reach the disk surface at radii where also the contrast between the emission feature and the dust continuum allows their detection.

6.3. Comparison to TTauri stars and HAeBe Stars

The results from the correlated flux allow a comparison to disks around other YSOs that have also been observed with VLTI/MIDI. Not only seem crystalline silicates be commonly present in protoplanetary disks, but for three intermediate-mass HAeBes stars van Boekel et al. (2004) found that the degree of crystallization within the disk depends on the distance from the central star. The inner parts of the disks are more crystalline than the outer disk regions. This can naturally be explained by assuming that in the inner disk regions where the disk has higher temperatures dust processing and annealing occurs and that over time crystalline particles are transported outwards. Not only for intermediate mass stars but also for the TTauri star RY Tau the same radial dependence of the crystallinity was observed (Schegerer et al. 2006). Thus, crystalline silicates should in general be more easily detectable in the correlated spectra of protoplanetary disks. For reasons mentioned in the previous section it seems thus surprising that the disk around FU Orionis does not seem to contain any detectable amount of crystalline dust.

As described in the introduction FUORs are believed to be low-mass or TTauri-like stars in a state of enhanced accretion. From sub-millimeter and millimeter observations Weintraub et al. (1991) concluded that FUORs are possibly in an evolutionary younger age than classical TTauri stars. This younger age is also supported by theoretical models where the protostellar disk is continuously replenished by a dusty envelope. This material infall on the disk can lead to thermal instabilities in the disk and thus provides a possible mechanism for explaining the observed outbursts Bell et al. (1995). The puzzling thing is now that apparently in the disk surrounding FU Ori the amorphous grains have already grown considerably. Hence, the disk can not be in its native dust composition and might already have a significant age. Furthermore, from the *Spitzer* FEPS (*Formation and Evolution of Planetary Systems*) legacy program it is known that apparently the amount of crystalline silicates in TTauri disks is not correlated with the average size of amorphous dust particles (Bouwman et al. 2006). Hence, crystalline dust particles are created in the *early* phases of disk evolution where the accretion rate and the disk temperature are thought to be higher. If thus the FUOR-phase is indeed common to most/all TTauri stars then the non-detection of crystalline particles cannot be explained in the current picture of protoplanetary disk evolution.

7. A Simple Disk Model

7.1. The SED

The present paper is more intended to show the observational results rather than to present a sophisticated disk model possibly able to match the observed SED and visibilities with highest accuracy. Thus, instead of applying a complex radiative transfer model we decided to use in a first step a simple analytical disk model. In this model the effective temperature and also the surface density are prescribed by the following broken power law distributions

$$T(r) = T_{1AU} \left(\frac{r}{1AU} \right)^{-q} \quad (6)$$

$$\Sigma(r) = \Sigma_0 \left(\frac{r}{r_0} \right)^{-p} \quad (7)$$

For the temperature law the temperature at 1 AU and the exponent q are free parameters. For the surface density the total disk mass M_D and the exponent p are free parameters. As the integrated surface density must equal the total mass of the disk the radial dependence of the surface density $\Sigma(r)$ can be computed. The shape of the total SED (and finally also the observed visibilities) require a double power-law to fit the data. At a radius of 3 AU the temperature and surface density distribution change. However, we made sure that for both parameters the transition was smooth and continuous. Figure 9 shows the SED and the resulting fit from the simple disk model. The model parameters are summarized in Table 7. Based on the value for the visual extinction A_V we interpolated the extinction for the other wavelengths following the findings of Mathis (1990). The disk inclination i was derived from the ellipses fitted to the FWHM of assumed Gaussian brightness distributions (see section 5.3.). For the position angle θ we used two values: One was also derived in section 5.3., and for the second one we fitted the disk model to the observed visibilities with θ being the only free parameter (see also section 7.2.).

It is clear that this simple approach is not able to reproduce all features of the SED (e.g., the weak silicate emission feature). For the moment, however, we restrict ourselves to this simple approach and, as mentioned above, a detailed modeling is left for further investigations. It is striking that rather high disk temperatures are required to fit the SED. In the inner 0.35 AU no dust can withstand the high temperatures >1500 K even on the disk surface and only the gaseous disk component can survive. It is interesting to note that the power law index of $q_1 = 0.75$ of the inner disk region equals exactly that what was derived in analytical disk models for geometrically flat, optically thick *passive* disks (e.g., Adams, Lada

& Shu 1987) as well as for flat, steady state, optically thick *accretion* disks (e.g., Pringle 1981). Thus, from the temperature distribution alone one can not distinguish between the two different cases (see also Kenyon & Hartmann 1987). However, in the context of FU Ori the passive disk model where the disk is merely re-processing radiation from the central star is unlikely and only an accretion disk model matches most observations (Hartmann & Kenyon 1996). A nice example is the recently detected magnetic field in the innermost regions of the disk surrounding FU Ori which can only be explained in the picture of a heavily accreting disk (Donati et al. 2005). As the disk temperature is directly related to the mass accretion rate \dot{M} in classical accretion disk models it is possible to derive the \dot{M} required to produce the observed high temperatures. Bell et al. (1997) analyzed the effective disk temperature and also the midplane temperature of an accretion disk as a function of the mass accretion rate. Figure 1 of their paper shows that one needs $\dot{M} \geq 10^{-5} M_{\odot}/\text{yr}$ to get close to the effective temperature we find in our model. Such high values for \dot{M} were also found by Hartmann & Kenyon (1996) and Lachaume et al. (2003). Due to the high accretion rate the midplane temperature of the disk in the inner ≈ 10 AU is even much higher than the effective disk temperature (Bell et al. 1997).

Concerning the temperature law farther out than 3 AU the value we adopt here for q_2 is in good agreement to what can be found in the literature for isothermal flared disks (Kenyon & Hartmann 1987). In their model the index value diverges from the flat solution where $q = 0.75$ at a certain point in the inner disk and approaches $q = 0.5$ for radii much larger than the stellar radius. At intermediate radii the temperature index might be approximated by values in between these most extreme cases depending on the actual flaring of the disk.

In summary, the temperature distribution indicates that in the innermost disk regions the disk luminosity is accretion dominated whereas further out it is irradiation dominated. This is expected for an active accretion disk since the luminosity released by accretion is a much steeper function of distance to the star than that by absorption of radiation from the central star and the hot innermost disk regions ($L_{\text{accretion}} \propto r^{-4}$, whereas $L_{\text{absorption}} \propto r^{-2}$, roughly).

7.2. Model visibilities

7.2.1. MIR results

For this simple disk model it is straightforward to compute the visibilities as a function of projected baseline and wavelength. Assuming that each part of the disk surface is emitting as a blackbody with an effective temperature $T(r)$ the corresponding total flux and visibility

for an axisymmetric face-on disk is given by (see also equations (2), (3), and following in Malbet et al. 2005):

$$F_\lambda = \frac{2\pi}{d^2} \int_{r_{min}}^{r_{max}} r B_\lambda(T(r)) dr \quad (8)$$

$$V_\lambda(B_P) = \frac{2\pi}{F_\lambda d^2} \int_{r_{min}}^{r_{max}} r B_\lambda(T(r)) J_0\left[\frac{2\pi}{\lambda} B_P \frac{r}{d}\right] dr \quad (9)$$

with F_λ being the flux, B_λ the Planck function, J_0 the zeroth-order Bessel function of the first kind, B_P the projected baseline and d the distance to the object.

Taking into account the inclination of the disk and the position angle as given in Table 7 we computed the corresponding visibilities for the three different baselines. The results for two different position angles are shown in Figure 10. In the upper panel the disk inclination and the position angle are derived from the ellipses fitting in section 5.3. In the lower panel the position angle was fitted to the observed visibilities with a least squares fit. While the ellipse fitting yielded a position angle of $109.1^\circ \pm 11.6^\circ$ a least square analysis leads to a value of $93.4^\circ \pm 6.8^\circ$. From the plots in Figure 10 one can see that changing the position angle mostly affects the visibility of the shortest baseline while the curves for the other baselines change only marginally.

Fitting the UT3-UT4 baseline proofs quite a challenge as the observed visibility is increasing over the $8-13\mu\text{m}$ wavelength interval while all other modeled visibilities are decreasing. Especially for this baseline better fits are expected from more sophisticated disk models. However, given the simplicity of the current models the fits seems in reasonable agreement with the observations. It clearly shows that interferometric measurements can put additional constraints on the structure and geometry of circumstellar disks that cannot be derived from SED fitting alone.

Interestingly, Malbet et al. (2005) were able to fit their NIR visibilities of FU Ori with a similar disk model and also with a disk and an embedded "hot spot". They concluded that the latter model was more likely based on statistical arguments. The major differences between their models and ours is that (1) they fit the SED with single power laws for the temperature neglecting the flux longwards of $20\mu\text{m}$ and (2) their best fits yield disk position angles of $47^\circ \pm 7^\circ$ and $8^\circ \pm 21^\circ$. The inclination angles ($55^\circ \pm 5^\circ$ and $48^\circ \pm 9^\circ$, respectively), are in good agreement with our value. In Figure 11 we compare both of their models to our observations. We find that both models fit the MIDI visibilities not as good as the model presented here. Even more we find that our MIR interferometric measurements rule out their first model of a simple accretion disk. This model predicts a higher visibility for the UT3-UT4 baseline than for the UT2-UT3 baseline which is not observed. The model with

an embedded "hot spot" in the accretion disk shows the right trend for the visibilities, but the values for the UT3-UT4 and UT2-UT4 baseline are higher than for our models which already give slightly too high values compared to the observations. The main reason for the higher visibilities resulting from the model applied by Malbet et al. (2005) is the single power law approach which provides less MIR flux compared to our models.

7.2.2. *NIR results*

We also compared our models to the measured NIR visibilities from Malbet et al. (2005). We restricted ourselves to those observations where the object was clearly resolved. The results are given in Table 8. Except for the observations done with north-west baseline of the Palomar Testbed Interferometer (PTI/NW) both of our models agree with the NIR visibilities within the error bars.

Concerning the predicted "hot spot" in the accretion disk (Malbet et al. 2005) our observations do not yield new insights into its nature as they do not have the required spatial resolution to confirm its existence. Also the calibrated phase of our observations do not contain any information on which basis we could speculate about this possible second companion.

8. Conclusions and Future Prospects

We presented the first multi-baseline MIR interferometric observations of FU Orionis with MIDI/VLTI. The findings can be summarized as follows:

1. FU Orionis was clearly resolved in the MIR with two VLTI baselines and marginally resolved with a third baseline indicating the presence of warm dusty material surrounding FU Ori out to several tens of AU.
2. The inclination and the position angle of the accretion disk can be inferred from multi-baseline measurements with MIDI/VLTI. Thus, the instrument provides means for deriving disk parameters that are otherwise only poorly constrained from models and SED fits.
3. The correlated flux indicates that 95% of the 8-13 μ m flux comes from within the inner 25AU of the disk for the shortest of our baselines while 65% of this flux arise from the inner 13AU for our longest baseline.

4. The shapes and strengths of the total 8-13 μ m spectrum and the (spatially resolved) correlated spectra indicate that most dust particles within the accretion disk are amorphous and already significantly larger than typical particles in the ISM.
5. No spectra, neither the total nor the spatially resolved correlated spectra bear significant traces of crystalline silicates. Given the high accretion rate and disk temperature of the system this is unexpected and requires further investigations.
6. The SED and the observed MIR visibilities can be fitted reasonably well with a simple analytical disk model prescribing a broken power law for the effective temperature distribution of the protoplanetary disk. Within the innermost 3AU the temperature decreases with $T \propto r^{-0.75}$, farther out the temperature goes with $T \propto r^{-0.53}$. The derived power law index for the inner regions is equal to what is derived theoretically for flat, steady state, optically thick accretion disks (Pringle 1981). For the outer disk region the derived value is in good agreement to what can be found for isothermal flared disks (Kenyon & Hartmann 1987).
7. Based on points 4. and 5. and recent spectroscopic observations of protoplanetary disks around TTauri stars and HAeBes it seems questionable that FU Ori is a very young classical TTauri star as the size of amorphous dust grains in combination with the non-detection of crystalline dust contradicts this assumption.
8. From the acquisition image N-band aperture photometry could be derived for the companion FU Ori S. It shows that this young K-type star has more relative MIR excess than FU Ori itself hinting at a circumstellar disk with larger flaring angle or smaller disk inclination.

Putting these results into context with other high spatial resolution studies of FU Ori and other FUORs we see that:

1. Most of the published NIR visibilities of FU Ori (Malbet et al. 2005) do agree with our newly derived disk models.
2. Our interferometric observations rule out one out of two disk models for FU Ori presented by Malbet et al. (2005). Due to the lack of sufficient spatial resolution the presence of the proposed second very close companion can neither be confirmed nor disproved with the current set of MIDI data.
3. In contrast to NIR interferometric observations of other FUORs (Millan-Gabet et al. 2006) our data do not seem to require the introduction of an extended dusty structure providing additional uncorrelated flux.

4. For the inner 3AU we require a significantly different disk model (e.g., $\Sigma \propto r^{-0.9}$, $T \propto r^{-0.75}$) to fit our visibilities and SED in comparison to what was found for the outbursting star V1647 Ori ($\Sigma \propto r^{-1.5}$, $T \propto r^{-0.53}$) (Ábrahám et al. 2006).

Although the present results provide important new insights into the FU Ori system new questions arose as well. Future investigations will include a more thorough and detailed modeling of the observations with numerical radiative transfer disk models. These models will not only need to consider the high accretion rates but also such effects as self-irradiation of the disk. It will be interesting to see whether these models are able to confirm the apparent rotation of the disk's position angle with wavelength and whether they can reproduce the increasing visibility curve for the UT3-UT4 baseline. Also, these disk models will have to reproduce the observed NIR and MIR visibilities simultaneously with higher accuracy than the current simple models are able to do. From the observational side re-measuring the UT3-UT4 baseline might be eligible and any other new baseline configuration will certainly help to constrain the disk geometry (especially the position angle) even better. Concerning the dust structure the lack of crystalline silicates needs to be analyzed in greater detail. Is it still just a contrast effect that we do not see any crystalline features in the spectra or are they simply not there? Eventually we will have to face the problem that currently all FUORs that have been observed with high spatial resolution techniques draw a rather inhomogeneous picture of the group. Apparently, some are still surrounded by nearby dense envelopes while for others the circumstellar disks suffice to explain the observations. However, even those disk-systems (i.e., FU Ori and V1647 Ori) seem to be different in terms of physical properties as different temperature and surface density profiles are derived.

Without any doubt interferometric observations of circumstellar disks in the NIR and MIR provide an unprecedented means for deriving geometrical disk properties and put new constraints on the physical (and also chemical) processes taking place within protoplanetary disks. And as more and more interferometric data of circumstellar disks are published our view on the cradle of planetary systems will be once more refined.

S. P. Quanz kindly acknowledges financial support by the German *Friedrich-Ebert-Stiftung*. Th. Henning and J. Bouwman acknowledge financial support by the EC-RTN on "The Formation and Evolution of Young Stellar Clusters" (HPRN-CT-2000-00155). We are most grateful to R. Köhler and F. Lahuis for their support during the data reduction and to R. Lachaume and F. Malbet for providing MIR data derived from their disk models (section 7.2.). We thank our anonymous referee for a detailed and thorough review that improved the manuscript. This research has made use of the SIMBAD database, operated at CDS, Strasbourg, France, and was partly based on observations made with the *Spitzer*

Space Telescope, which is operated by the Jet Propulsion Laboratory, California Institute of Technology, under NASA contract 1407.

REFERENCES

Adams, F.C., Lada, C.J., Shu, F.H.: *ApJ* **312**, 788 (1987)

Ábrahám, P., Mosoni, L., Henning, Th., Kóspál, Á., Leinert, Ch., Quanz, S.P., Ratzka, Th.: *A&A* **449**, L13 (2006)

Bell, K.R., Lin, D.N.C., Hartmann, L.W., Kenyon, S.J.: *ApJ* **444**, 376 (1995)

Bell, K.R., Cassen, P.M., Klahr, H.H., Henning, Th.: *ApJ* **486**, 372 (1997)

Bonnell, I. & Bastien, B.: *ApJ* **401**, L31 (1992)

Bouwman, J., Meeus, G., de Koter, A., Hony, S., Dominik, C., Waters, L.B.F.M.: *A&A* **375**, 950 (2001)

Bouwman, J., Henning, Th., et al. (2006, in preparation)

Clarke, C., Lodato, G., Melnikov, S.Y., Ibrahimov, M.A.: *MNRAS* **361**, 942 (2005)

Donati, J.-F., Paletou, F., Bouvier, J., Ferreira, J.: *Nature* **438**, 466 (2005)

Dorschner, J., Begemann, B., Henning, Th., Jäger, C., and Mutschke, H.: *A&A* **300**, 503 (1995)

Ducati, J.R.: VizieR On-line Data Catalogue: II/237 (2002)

Dullemond, C.P., Apai, D. & Walch, S.: *A&A* **640**, L78 (2006)

Gail, H.-P.: *A&A* **413**, 571 (2004)

Gail, H.-P.: *A&A* **378**, 192 (2001)

Gullbring, E., Hartmann, L., Briceno, C., Calvet, N.: *ApJ* **492**, 323 (1998)

Haisch, K.E.Jr., Lada, E.A., Lada, C.J.: *AJ* **121**, 1512 (2001)

Hanner, M.S., Brooke, T.Y., Tokunaga, A.T.: *ApJ* **502**, 871 (1998)

Hartmann, L. & Kenyon, S.J.: *ARA&A* **34**, 207 (1996)

Henning, Th., Mutschke, H. & Jäger, C. (2006), In *Astrochemistry: Recent Successes and Current Challenges*, (D.C. Lis, G.A. Blake & E. Herbst, eds), Proceedings IAU Symposium 231

Herbig, G.H., Petrov, P.P., Duemmler, R.: *ApJ* **595**, 384 (2003)

Herbig, G.H.: *ApJ* **217**, 693 (1977)

Higdon, S.J.U., Devost, D., Higdon, J.L., Brandl, B.R., Houck, J.R., et al.: *PASP* **116**, 975 (2004)

Jäger, C., Molster, F.J., Dorschner, J., et al.: *A&A* **339**, 904 (1998)

Kenyon, S.J., Hartmann, L.: *ApJ* **323**, 714 (1987)

Kenyon, S.J., Hartmann, L. & Hewett, R.: *ApJ* **325**, 231 (1988)

Lachaume, R.: *A&A* **422**, 171 (2004)

Lachaume, R., Malbet, F., Monin, J.-L.: *A&A* **400**, 185 (2003)

Leinert, Ch., van Boekel, R. et al.: *A&A* **537**, 423 (2004)

Lodato, G. & Clarke, C.J.: *MNRAS* **353**, 841 (2004)

Malbet, F., Lachaume, R., Berger, J.-P., Colavita, M. M., di Folco, E., Eisner, J. A., Lane, B. F., Millan-Gabet, R., Segransan, D., Traub, W. A.: *A&A* **437**, 627 (2005)

Mathis, J.S.: *ARA&A* **28**, 37 (1990)

Mennesson, B., Koresko, C., Creech-Eakman, M. J., Serabyn, E., Colavita, M. M., Akeson, R., Appleby, E., Bell, J., Booth, A., Crawford, S., et al.: *ApJ* **634**, L169 (2005)

Men'shchikov, A.B. & Henning, Th.: *A&A* **879**, 318 (1997)

Millan-Gabet, R., Monnier, J.D., Akeson, R.L., Hartmann, L., Berger, J.-P., et al.: astro-ph/0512230 (accepted by *ApJ*)

Min, M., Hovenier, J.W. & de Koter, A.: *A&A* **432**, 909 (2005)

Molster, F. & Kemper, C.: *Space Science Reviews* **119**, 3 (2005)

Peeters, E., Hony, S., Van Kerckhoven, C., et al.: *A&A* **390**, 1089 (2002)

Pringle, J.E.: *ARA&A* **19**, 137 (1981)

Przygoda, F.: PhD Thesis at the University of Heidelberg (2004)

Schegerer, A., Wolf, S., et al. (2006, in preparation)

Reipurth, B. & Aspin, C.: *ApJ* **608**, L65 (2004)

Servoin, J.L. & Piriou, B.: *phys. stat. sol.* **55**, 677 (1973)

Spitzer, W.G. & Kleinman, D.A.: *Physical Review* **121**, 1324 (1960)

van Boekel, R., Min, M., Leinert, Ch., Waters, L.B.F.M., Richichi, A., Chesneau, O., Dominik, C., Jaffe, W., et al.: *Nature* **432**, 479 (2004)

van den Ancker, M.E., Bouwman, J., Wesselius, P.R., et al.: *A&A* **357**, 325 (2000)

van Diedenhoven, B., Peeters, E., Van Kerckhoven, C., et al.: *ApJ* **611**, 928 (2004)

Voshchinnikov, N. V., Il'in, V. B., Henning, Th., Dubkova, D. N.: *A&A* **445**, 167 (2006)

Wang, H., Apai, D., Henning, Th., Pascucci, I.: *ApJ* **601**, L83 (2004)

Weintraub, D.A., Sandell, G., Duncan, W.D.: *ApJ* **382**, 270 (1991)

Welin, G.: *A&A* **12**, 312 (1971)

Table 1. Journal of MIDI observations of FU Orionis and the calibrators used for the data reduction.

Date	Object	Projected Baseline	Position Angle	Comment
31.10.2004	FU Ori	44.56 m (UT2-UT3)	46.54°	-
	HD37160			Calibrator ^a
02.11.2004	FU Ori	86.25 m (UT2-UT4)	84.24°	-
	HD 31421			Calibrator
	HD 37160			Calibrator
	HD 50778			Calibrator
04.11.2004	FU Ori	56.74 m (UT3-UT4)	106.64°	-
	HD 25604			Calibrator
	HD 20644			Calibrator
	HD 37160			Calibrator
	HD 50778			Calibrator
29.12.2004	FU Ori	44.80 m (UT2-UT3)	46.61°	-
	HD 37160			Calibrator
	HD 94510			Calibrator ^a

^aObserved twice that night.

Table 2. Photometric values for the FU Ori system. J to L' are taken from Reipurth & Aspin (2004), N-band values are derived from MIDI 8.7 μ m acquisition images. The errors for the N-band fluxes are standard deviations based on measurements of three acquisition images. Two were taken on 31.10.2004 and one on 02.11.2004.

	FU Ori	FU Ori S
J [mag]	6.30 \pm 0.03	10.75 \pm 0.23
H [mag]	5.64 \pm 0.05	9.92 \pm 0.21
K' [mag]	5.25 \pm 0.02	9.15 \pm 0.15
L' [mag]	4.18 \pm 0.04	8.09 \pm 0.16
N [mag]	2.75 \pm 0.19	5.28 \pm 0.11

Table 3. Dust species used in the dust model. Apart from the name, the chemical formula, the shape and also the reference to laboratory measurements for the optical properties are given. Mie-theory was used to calculate the opacities for the homogeneous spheres whereas for the inhomogeneous spheres we used the distribution of hollow spheres given by Min et al. (2005) to simulate grains that are not perfectly symmetric. *References:* (1) Dorschner et al. (1995), (2) Servoin & Piriou (1973), (3) Jäger et al. (1998), (4) Spitzer & Kleinman (1960).

Species	Chemical Formula	Shape	Ref
Amorphous Olivine	MgFeSiO_4	Homogeneous	(1)
Amorphous Pyroxene	$\text{MgFeSi}_2\text{O}_6$	Homogeneous	(1)
Crystalline Forsterite	Mg_2SiO_4	Inhomogeneous	(2)
Crystalline Enstatite	MgSiO_3	Inhomogeneous	(3)
Amorphous Silica	SiO_2	Inhomogeneous	(4)

Table 4. Possible dust composition for the observed $10\mu\text{m}$ silicate feature as derived with our dust model. The mass fraction of three grain sizes for different dust species is given.

	0.1 μm	1.5 μm	6.0 μm	Total
Amorphous Olivine	0.17	< 0.01	0.18	0.35
Amorphous Pyroxene	< 0.01	0.07	0.57	0.64
Crystalline Silicates ^a	< 0.01	< 0.01	< 0.01	< 0.01

^aForsterite and Enstatite

Table 5. Calibrated visibilities for FU Ori observed with three different baselines. The errors are standard deviations resulting from calibrations with different calibrator stars for each night.

Wavelength [μm]	V [UT2-UT3 ^a]	V [UT2-UT4 ^b]	V [UT3-UT4 ^c]
12.95	0.98 \pm 0.02	0.60 \pm 0.02	0.84 \pm 0.02
12.83	0.93 \pm 0.02	0.61 \pm 0.03	0.83 \pm 0.02
12.70	0.94 \pm 0.03	0.63 \pm 0.03	0.84 \pm 0.02
12.57	0.96 \pm 0.02	0.62 \pm 0.02	0.84 \pm 0.02
12.44	0.96 \pm 0.02	0.62 \pm 0.02	0.81 \pm 0.02
12.31	0.94 \pm 0.02	0.60 \pm 0.01	0.81 \pm 0.02
12.17	0.92 \pm 0.01	0.61 \pm 0.02	0.79 \pm 0.02
12.03	0.94 \pm 0.02	0.61 \pm 0.02	0.81 \pm 0.02
11.89	0.93 \pm 0.03	0.62 \pm 0.02	0.79 \pm 0.02
11.75	0.94 \pm 0.03	0.62 \pm 0.01	0.78 \pm 0.02
11.60	0.94 \pm 0.03	0.63 \pm 0.01	0.77 \pm 0.02
11.45	0.91 \pm 0.02	0.63 \pm 0.01	0.79 \pm 0.02
11.30	0.94 \pm 0.03	0.62 \pm 0.01	0.78 \pm 0.02
11.14	0.92 \pm 0.03	0.62 \pm 0.01	0.76 \pm 0.02
10.98	0.93 \pm 0.02	0.62 \pm 0.01	0.77 \pm 0.02
10.82	0.92 \pm 0.02	0.62 \pm 0.01	0.76 \pm 0.01
10.66	0.92 \pm 0.02	0.62 \pm 0.01	0.75 \pm 0.01
10.49	0.91 \pm 0.01	0.62 \pm 0.01	0.75 \pm 0.02
10.32	0.92 \pm 0.02	0.63 \pm 0.01	0.75 \pm 0.02
10.15	0.92 \pm 0.01	0.63 \pm 0.01	0.75 \pm 0.02
9.97	0.94 \pm 0.02	0.65 \pm 0.01	0.73 \pm 0.01
9.80	0.97 \pm 0.02	0.64 \pm 0.01	0.73 \pm 0.01
9.62	0.97 \pm 0.03	0.64 \pm 0.01	0.74 \pm 0.01
9.43	0.93 \pm 0.02	0.61 \pm 0.01	0.76 \pm 0.02
9.25	0.93 \pm 0.01	0.67 \pm 0.01	0.76 \pm 0.02
9.06	0.93 \pm 0.01	0.69 \pm 0.01	0.74 \pm 0.02
8.86	0.94 \pm 0.01	0.69 \pm 0.01	0.74 \pm 0.02
8.67	0.95 \pm 0.01	0.70 \pm 0.01	0.73 \pm 0.02
8.47	0.95 \pm 0.01	0.70 \pm 0.01	0.74 \pm 0.02
8.27	0.94 \pm 0.01	0.73 \pm 0.01	0.73 \pm 0.01

Table 5—Continued

Wavelength [μm]	<i>V</i> [UT2-UT3 ^a]	<i>V</i> [UT2-UT4 ^b]	<i>V</i> [UT3-UT4 ^c]

^aProjected Baseline: 44.56 m, Position Angle: 46.54°

^bProjected Baseline: 86.25 m, Position Angle: 84.24°

^cProjected Baseline: 56.74 m, Position Angle: 106.64°

Table 6. *Upper half*: Derived FWHM (in AU) of Gaussian brightness distributions for the three baselines and three wavelengths using equation 2. The distance to FU Ori is assumed to be 450 pc. *Lower half*: Parameters of best ellipses fitted to the data for the three considered wavelengths.

	9.0 μm	11.0 μm	12.5 μm
UT2-UT3 (44.56 m)	$2.47^{+0.40}_{-0.46}$	$3.27^{+0.67}_{-0.82}$	$3.43^{+0.81}_{-1.02}$
UT2-UT4 (86.25 m)	$3.25^{+0.24}_{-0.25}$	$4.34^{+0.07}_{-0.08}$	$4.93^{+0.17}_{-0.17}$
UT3-UT4 (56.74 m)	$4.19^{+0.28}_{-0.30}$	$5.00^{+0.35}_{-0.37}$	$4.83^{+0.43}_{-0.46}$
Semimajor axis a [AU]	2.28	2.51	2.54
Semiminor axis b [AU]	1.21	1.54	1.42
Ellipse area [AU ²]	8.67	12.14	11.33
Position angle θ^{a}	122.2°	111.1°	93.9°
Inclination i^{b}	58.0°	52.2°	56.0°

^aPosition of a measured from north eastwards

^bAssuming an underlying circular disk

Table 7. Parameters of the simple disk model used to fit the SED. The upper part of the table gives the parameters for the inner 3 AU. Farther out in the disk the temperature and surface density follow distributions defined by the parameters in the lower part of the table.

Parameter	Variable	Value
Inner disk radius	R_{in}	$5.5 R_{\odot}$
Outer disk radius	R_{out}	100 AU
Disk inclination ^a	i	55.4°
Disk position angle ^b	θ	109.1° ^a / 93.4° ^c
Extinction	A_V	2.6
Temperature at 1 AU	$T_{1AU,1}$	670 K
Power law index for temperature	$q1$	-0.75
Power law index for surface density	$p1$	-0.9
Disk mass	$M_{D,1}$	$0.03 M_{\odot}$
Temperature at 1 AU	$T_{1AU,2}$	550 K
Power law index for temperature	$q2$	-0.53
Power law index for surface density	$p2$	-1.4
Disk mass	$M_{D,2}$	$0.01 M_{\odot}$

^aAs derived in section 5.3.

^bOnly required for visibility computation

^cResulting from χ^2 -fit

Table 8. Comparison of observed NIR square visibilities from Malbet et al. (2005) to our disk model with two different position angles. The observations were carried out with different baselines at the Palomar Testbed Interferometer (PTI) and the Very Large Telescope Interferometer (VLTI).

Interferometer	Filter	Baseline [m]	Pos. Angle [deg]	V^2 (observed)	V^2 (model) ^a
PTI/NS	H	103.7	61.8	0.83 ± 0.04	0.80 / 0.82
PTI/NW	H	85.6	14.1	0.79 ± 0.05	0.92 / 0.94
PTI/NS	K	102.7	63.6	0.72 ± 0.08	0.78 / 0.80
PTI/NW	K	84.2	14.0	0.79 ± 0.05	0.91 / 0.93
PTI/SW	K	82.5	-55.6	0.82 ± 0.08	0.85 / 0.87
VLTI/UT1-UT3 ^b	K	89.6	54.2	0.87 ± 0.05	0.83 / 0.85

^aFor two different position angles: 109.1° / 93.4°

^bVINCI data

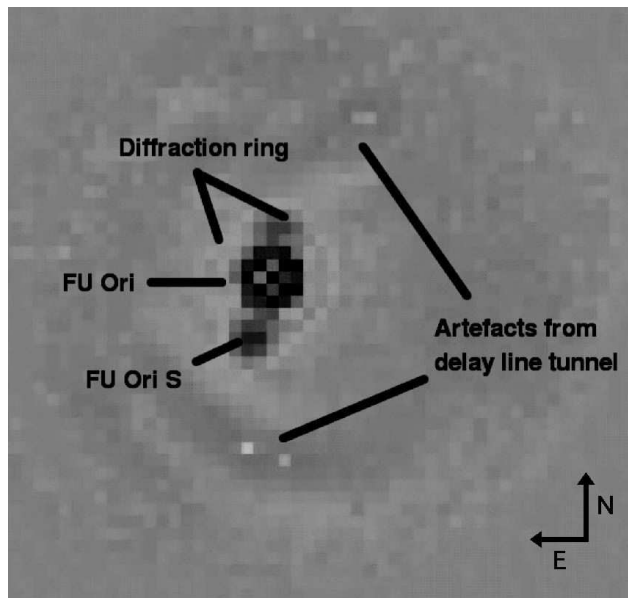


Fig. 1.— FU Ori and FU Ori S as seen in the MIDI acquisition images at $8.7\mu\text{m}$. The image was taken with UT3 the 31st of October 2004 using the AO-system MACAO (north is up, east to the left).

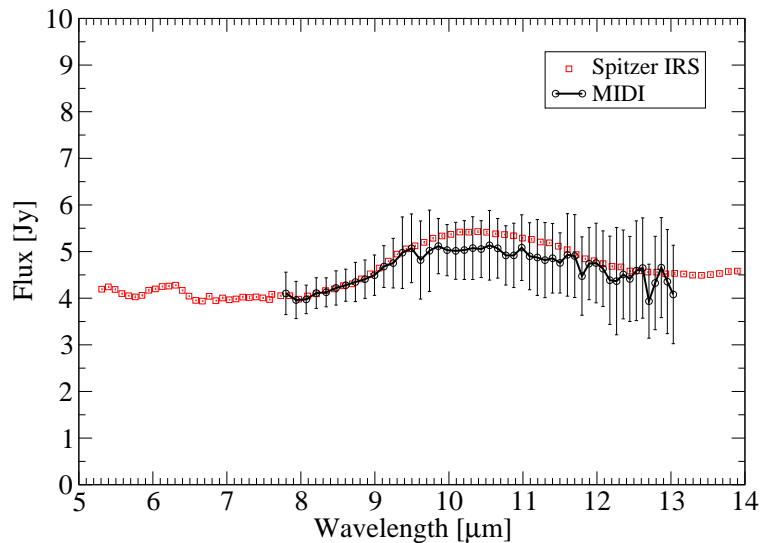


Fig. 2.— MIR spectrum of FU Ori from $5.3-14\mu\text{m}$. Data from the MIDI observations (dots with solid line) range from $8-13\mu\text{m}$. They agree within the error bars with *Spitzer IRS* data (squares). The errors for Spitzer are smaller than the symbols and are not shown. The larger MIDI errors arise from averaging six independently calibrated measurements (3 nights and 2 telescopes each night). The observed silicate feature is rather flat and broad.

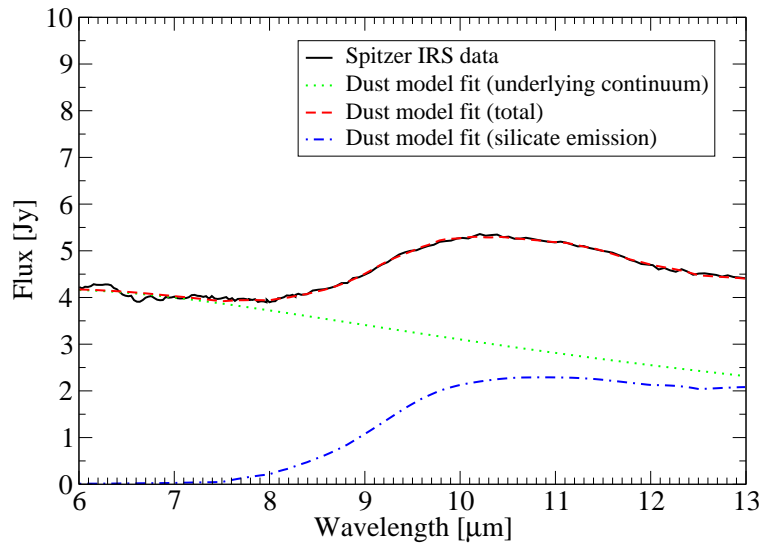


Fig. 3.— MIR spectrum of FU Ori and the resulting dust model fit. The *Spitzer* spectrum (black solid line) can be fitted quite well with the dust composition given in Table 4. The dotted line shows the contribution of the underlying continuum, the dash-dotted line shows the silicate emission and the grey dashed line shows the sum of both, i.e. the total flux, which is hardly distinguishable from the observed spectrum.

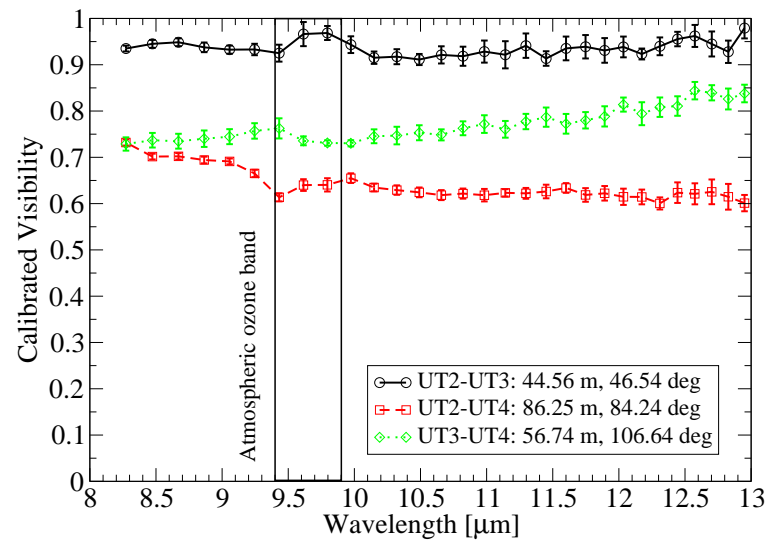


Fig. 4.— Calibrated Visibilities of FU Ori for three different baselines.

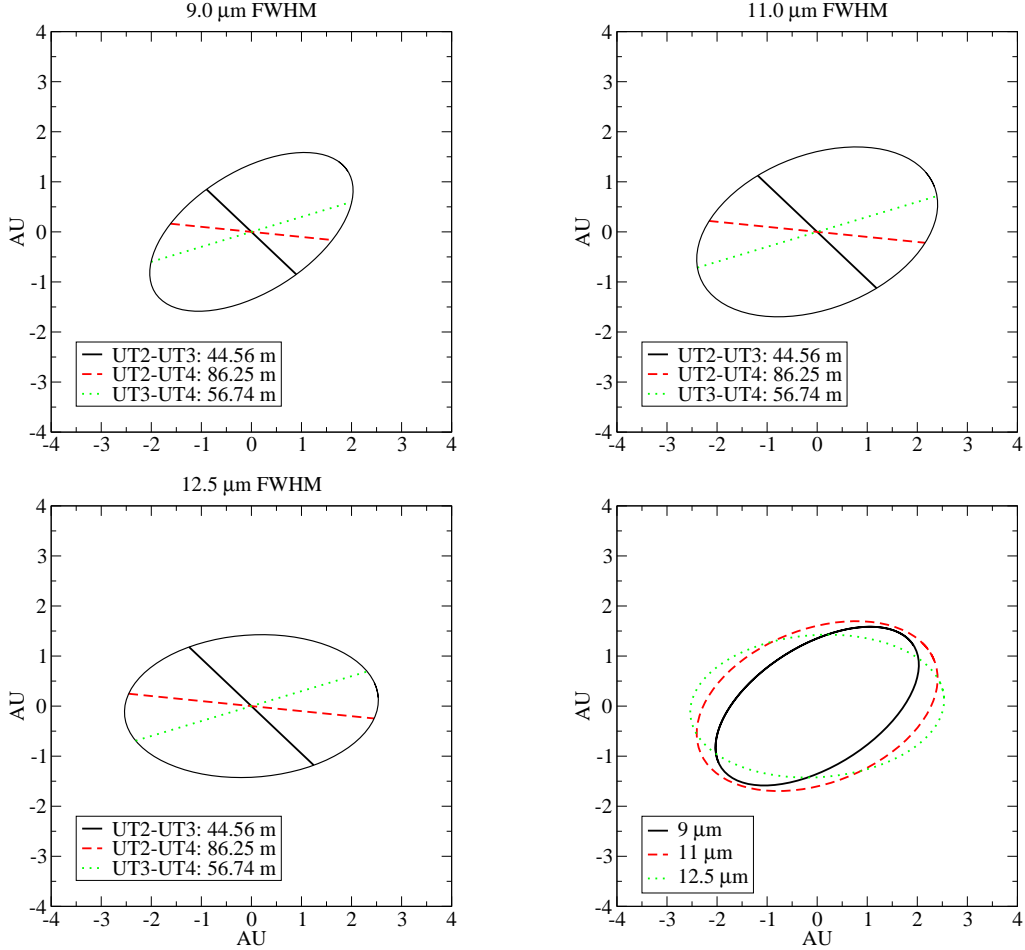


Fig. 5.— Sizes and orientation of the emitting regions on the sky for different wavelengths (9.0 μm (upper left), 11.0 μm (upper right) and 12.5 μm (lower left)). The sizes correspond to FWHM of assumed Gaussian brightness distributions and are given in Table 6. The resulting best fit ellipses for each wavelength are overplotted and combined in a fourth plot (lower right). The center of the plots corresponds to the position of FU Ori and north is up and east to the left.

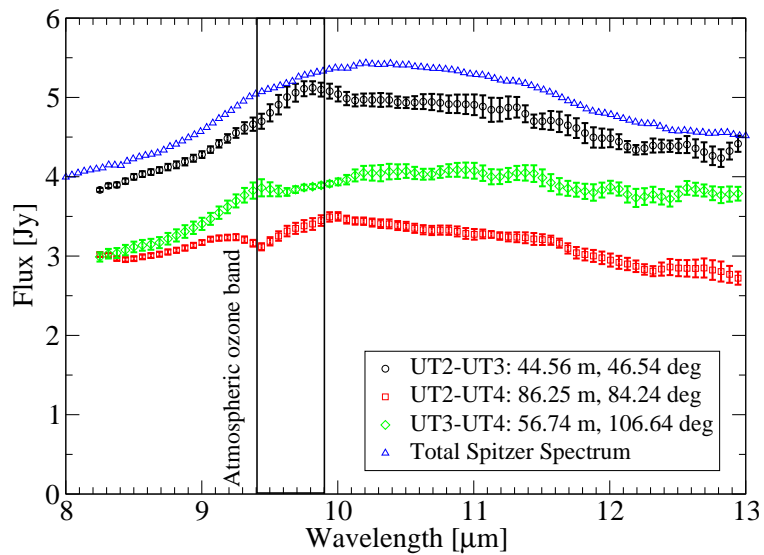


Fig. 6.— Observed correlated flux for the three different baselines and position angles.

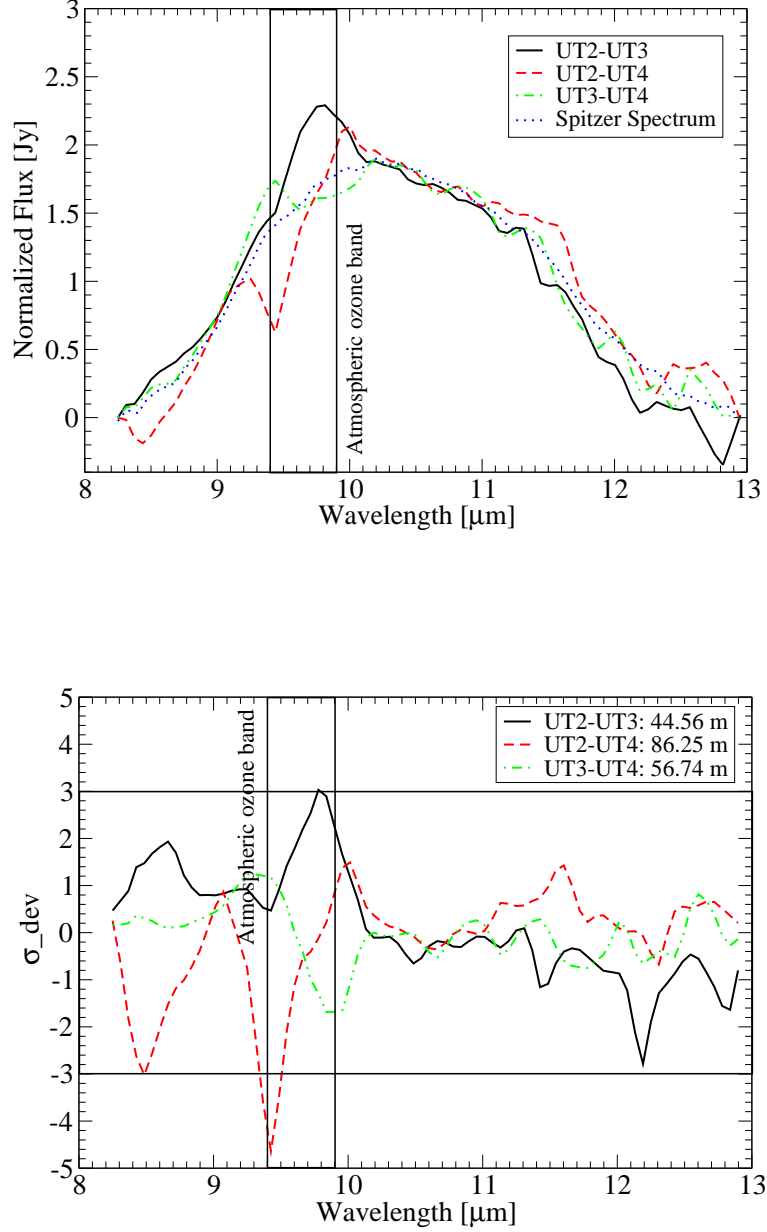


Fig. 7.— *Upper Panel:* Continuum subtracted and normalized correlated spectra for the three different baselines and the normalized total spectrum. For clarity the errorbars have not been overplotted. They equal those of Figure 6. *Lower Panel:* Variations of the normalized correlated spectra with respect to the normalized total *Spitzer* spectrum in units of error. It shows that most variations are clearly below the 3σ threshold, indicating that the shape of the correlated spectra equals that of the total spectrum.

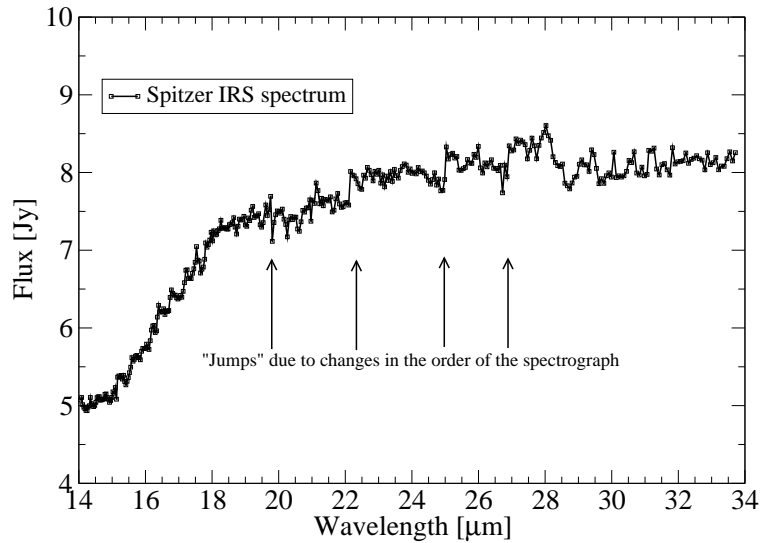


Fig. 8.— *Spitzer* MIR spectrum from 14-34 μ m. The spectrum was smoothed by a factor of three. The typical errors are smaller than the size of the symbols. Similar to the shorter wavelength spectrum in Figure 2 this spectrum appears rather smooth without any striking features. The arrows indicate where the order of the spectrograph is changing leading to variations in the detected flux (approximately at 19.6, 22.1, 25.0, and 26.7 μ m). Although the weak peak around 27.7-27.8 μ m can theoretically be attributed to the presence of forsterite particles their detection seems questionable as the normally stronger emission bands at 23.9 and 33.8 μ m is clearly not seen.

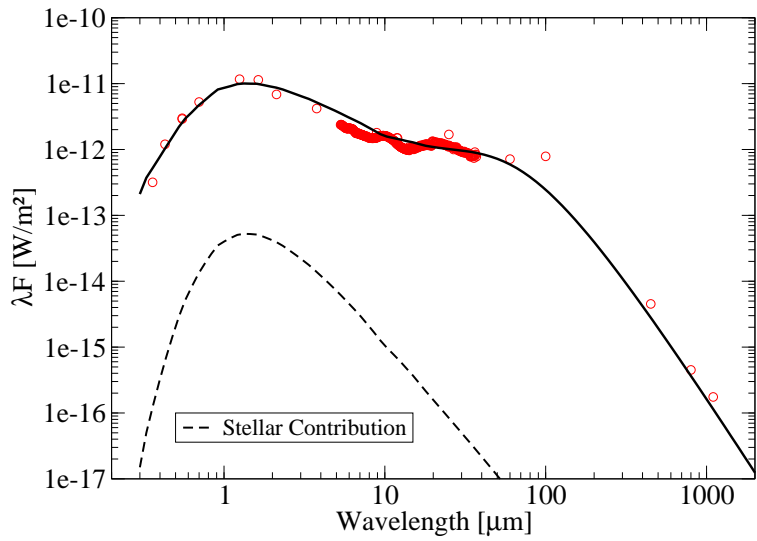


Fig. 9.— SED fit of a geometrically thin, optically thick accretion disk model. The disk parameters are shown in Table 7. The contribution of the central star (in this case we assume $T_{eff} = 3700 K$, $R_{star} = 2.5R_{\odot}$) can be neglected. Although simple, the disk model agrees reasonably well with the observed fluxes for most wavelength regimes. The data points were taken from Clarke et al. (2005) (U,B,V,R), Przygoda (2004) (8.9 μ m, 11.9 μ m), Reipurth & Aspin (2004) (J, H, K, L), Weintraub et al. (1991) (450 μ m, 850 μ m, 1.3mm), *Spitzer IRS* data archive (MIR Spectrum) and *IRAS* data archive (12 μ m, 25 μ m, 60 μ m, 100 μ m).

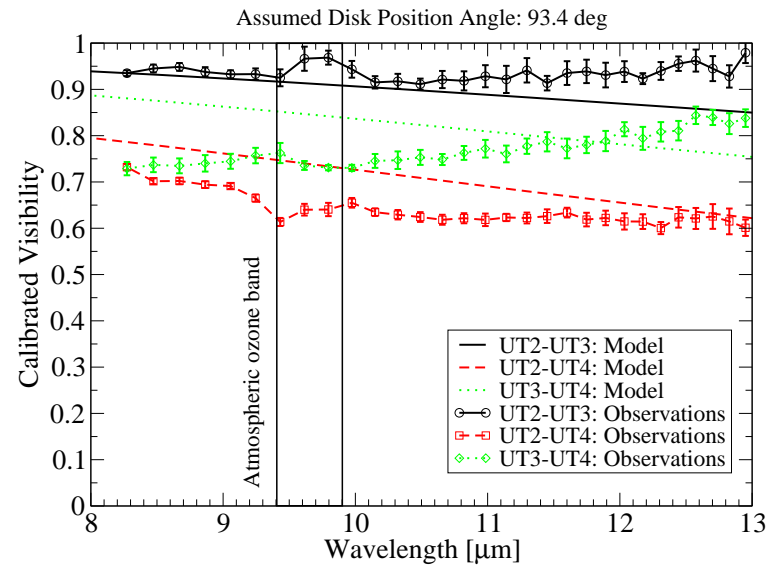
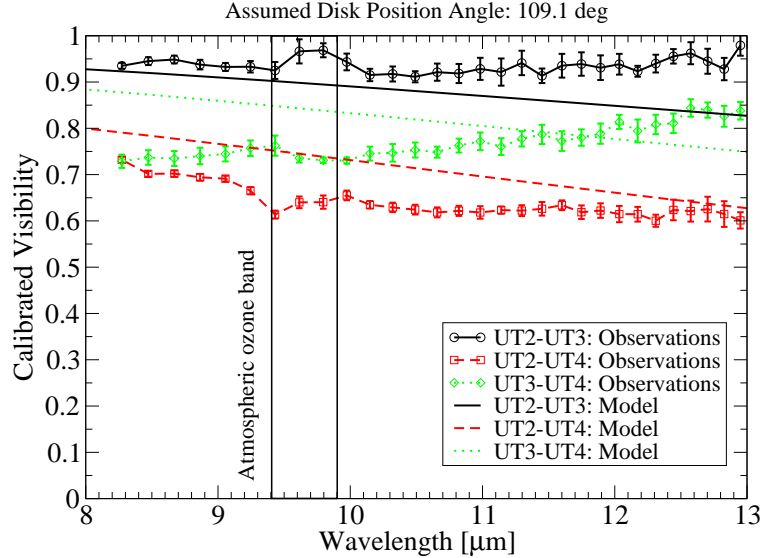


Fig. 10.— MIR visibilities derived from the simple disk model in comparison to the observations. The baselines and projection angles correspond to those given in Table 1. The disk position angle was assumed to be 109.1° in the upper panel and 93.4° in the lower panel. Changing the position angle has the biggest impact on the visibilities of the shortest baseline. Apparently, both models do show the right trend but they can not account for increasing visibilities.

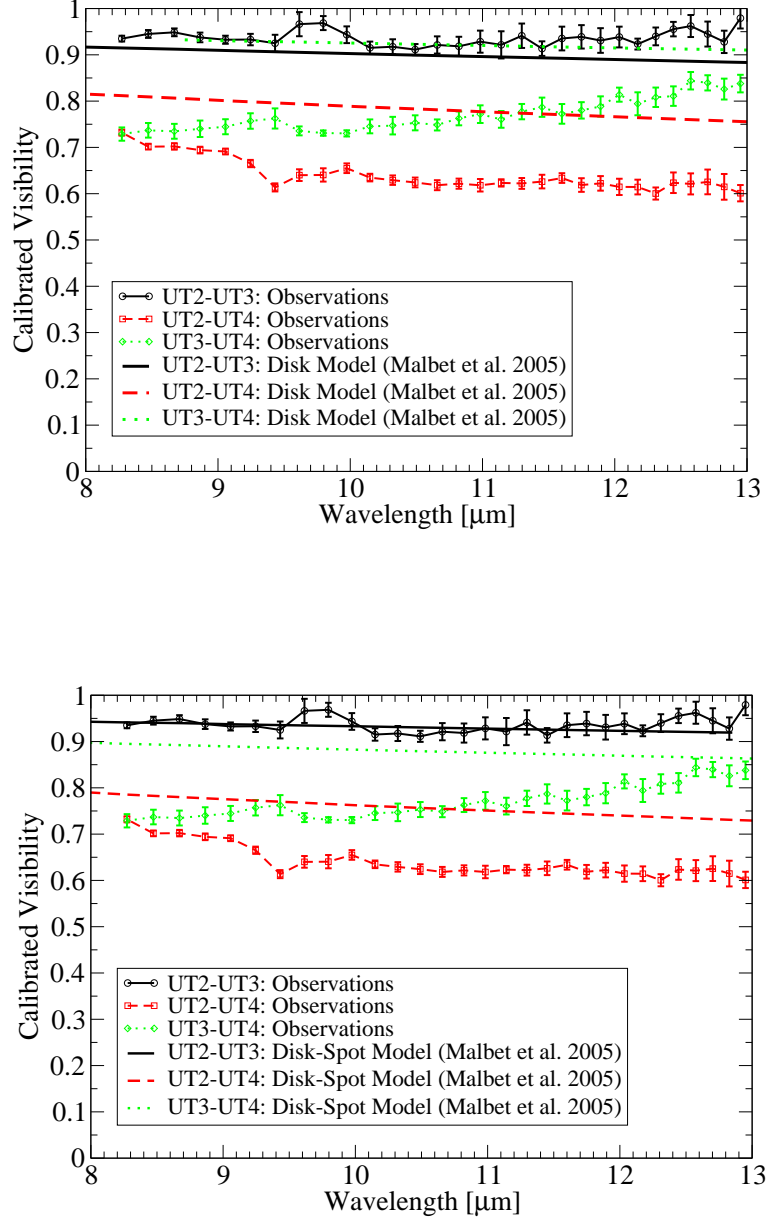


Fig. 11.— MIR visibilities derived from models for FU Ori presented in Malbet et al. (2005) in comparison to the observations. *Upper Panel:* Model consisting of a simple accretion disk. This model can be ruled out by our observations as it predicts higher visibilities for the UT3-UT4 baseline than for the UT2-UT3 baseline which is not observed. *Lower Panel:* Model consisting of an accretion disk and an embedded "hot spot". This model shows the right trend but does not fit the observations as good as the models presented in this paper.